LETTERS

A microRNA polycistron as a potential human oncogene

Lin He[1]*, J. Michael Thomson[2]*, Michael T. Hemann[1], Eva Hernando-Monge[4], David Mu[1], Summer Goodson[2], Scott Powers[1], Carlos Cordon-Cardo[4], Scott W. Lowe[1], Gregory J. Hannon[1] & Scott M. Hammond[2,3]

To date, more than 200 microRNAs have been described in humans; however, the precise functions of these regulatory, non-coding RNAs remains largely obscure. One cluster of microRNAs, the *mir-17–92* polycistron, is located in a region of DNA that is amplified in human B-cell lymphomas[1]. Here we compared B-cell lymphoma samples and cell lines to normal tissues, and found that the levels of the primary or mature microRNAs derived from the *mir-17–92* locus are often substantially increased in these cancers. Enforced expression of the *mir-17–92* cluster acted with *c-myc* expression to accelerate tumour development in a mouse B-cell lymphoma model. Tumours derived from haematopoietic stem cells expressing a subset of the *mir-17–92* cluster and *c-myc* could be distinguished by an absence of apoptosis that was otherwise prevalent in *c-myc*-induced lymphomas. Together, these studies indicate that non-coding RNAs, specifically microRNAs, can modulate tumour formation, and implicate the *mir-17–92* cluster as a potential human oncogene.

MicroRNAs (miRNAs) have emerged relatively recently as a new class of small, non-coding RNAs that regulate gene expression. Nascent primary miRNA transcripts (pri-miRNAs) are processed sequentially by two RNase III enzymes, Drosha and Dicer[2,3], to yield mature miRNAs, ranging from 18 to 24 nucleotides (nt) in length. miRNAs are incorporated into the RNA interference (RNAi) effector complex, RISC, and target specific messenger RNAs for translational repression or mRNA cleavage[4–6]. Although hundreds of miRNAs have been cloned and/or predicted, only a handful have been functionally characterized. For example, lin-4 and let-7 regulate the timing of larval development in *C. elegans*[7,8]. Left/right asymmetric gene expression in *C. elegans* chemosensory neurons is controlled by lsy-6 and miR-273 (refs 9, 10). Bantam stimulates cell growth and prevents apoptosis in *Drosophila*[11], and miR-181 potentiates B-cell differentiation in mammals[12]. These findings, in combination with computational target predictions, are consistent with miRNAs regulating a broad spectrum of physiological and developmental processes.

Microarray-based expression studies have indicated specific alterations in human miRNA expression profiles that correlate with particular tumour phenotypes (J.M.T. and S.M.H., unpublished data). Among those that show altered expression, the *mir-17–92* cistron is located at 13q31, a genomic locus that is amplified in cases of diffuse large B-cell lymphoma, follicular lymphoma, mantle cell lymphoma, primary cutaneous B-cell lymphoma and several other tumour types[1,13]. There are only two annotated genes in the epicentre of this amplicon, *c13orf25* and *GPC5*. Previous studies have shown that *c13orf25* is the only one of the two genes for which increased expression correlates with the presence of the amplicon[1]. Therefore, *c13orf25* had been implicated as a target of the 13q31 amplicon[1]. It is unlikely that *c13orf25* actually encodes a protein, as predicted open reading frames (ORFs) encode only short peptides (<70 amino acids), which are not conserved in closely related species. Instead, the *c13orf25* transcript appears to be the functional precursor of a series of seven microRNAs: miR-17-5p, miR-17-3p, miR-18, miR-19a, miR-20, miR-19b-1 and miR-92-1 (Fig. 1a). Additionally, this cluster is related to the homologous *mir-106a–92* cluster on chromosome X and the *mir-106b–25* cluster on chromosome 7 (ref. 14; Fig. 1a). Alignment of the human *c13orf25* locus and its murine orthologue revealed extensive sequence conservation only within the *mir-17–92* polycistron and its immediate flanking sequence. Several of the expressed-sequence-tags (ESTs) derived from *c13orf25* and its mouse orthologue terminate at the 3′ end of *mir-17–92* cluster, consistent with the presence of a Drosha processing site at this location (Fig. 1b).

A principal consequence of 13q31-q32 amplification could be an increase in the abundance of mature miRNA species from the *mir-17–92* cluster. We acquired four cell lines previously described as carrying amplifications in the 13q31-q32 region[1] and confirmed the gene dosage increase at the *c13orf25* locus in three of those cell lines using quantitative polymerase chain reaction (PCR) analysis. The abundance of 191 mature miRNAs was assessed in these four cell lines and compared to normal B-cells, and to five leukaemia and lymphoma cell lines lacking the amplicon (Fig. 1c and Supplementary Fig. 1). Using a significance analysis of microarrays (SAM) analysis[15], we identified six miRNAs for which high-level expression correlated with increased gene dosage of *c13orf25* (see Supplementary Table 1). Five were from the *mir-17–92* cistron, and the sixth, miR-106a, was identified as a probable result of cross-hybridization to miR-17-5p, from which it differs at only two terminal nucleotides (Fig. 1c). This hypothesis is supported by the observation that the *mir-106a–92* locus does not show copy number alterations in these cell lines (not shown). In each cell line, expression levels correlated with the copy number of the *mir-17–92* locus (Fig. 1c, lower panel).

We also examined the expression of pri-*mir-17–92* in a series of human tumour samples comprising both lymphomas and colorectal carcinomas. Of 46 lymphoma samples, including 13 diffuse large B-cell lymphomas and 6 follicular lymphomas, we saw significant (greater than fivefold) overexpression of pri-*mir-17–92* in 65% of the samples. Considering all of the B-cell lymphoma samples analysed, the average increase in pri-miRNA expression was about tenfold (Fig. 1d). In contrast, colorectal carcinomas rarely showed overexpression of the pri-miRNA. Increases in expression from this locus were less common (15% of samples showed greater than fivefold

[1]Cold Spring Harbor Laboratory, Watson School of Biological Sciences, 1 Bungtown Road, Cold Spring Harbor, New York 11724, USA. [2]Department of Cell and Developmental Biology and [3]Lineberger Comprehensive Cancer Center, University of North Carolina, Chapel Hill, North Carolina 27599, USA. [4]Memorial Sloan-Kettering Cancer Center, Division of Molecular Pathology, Memorial Sloan-Kettering Cancer Center, 1275 York Ave, New York, New York 10021, USA.
*These authors contributed equally to this work.

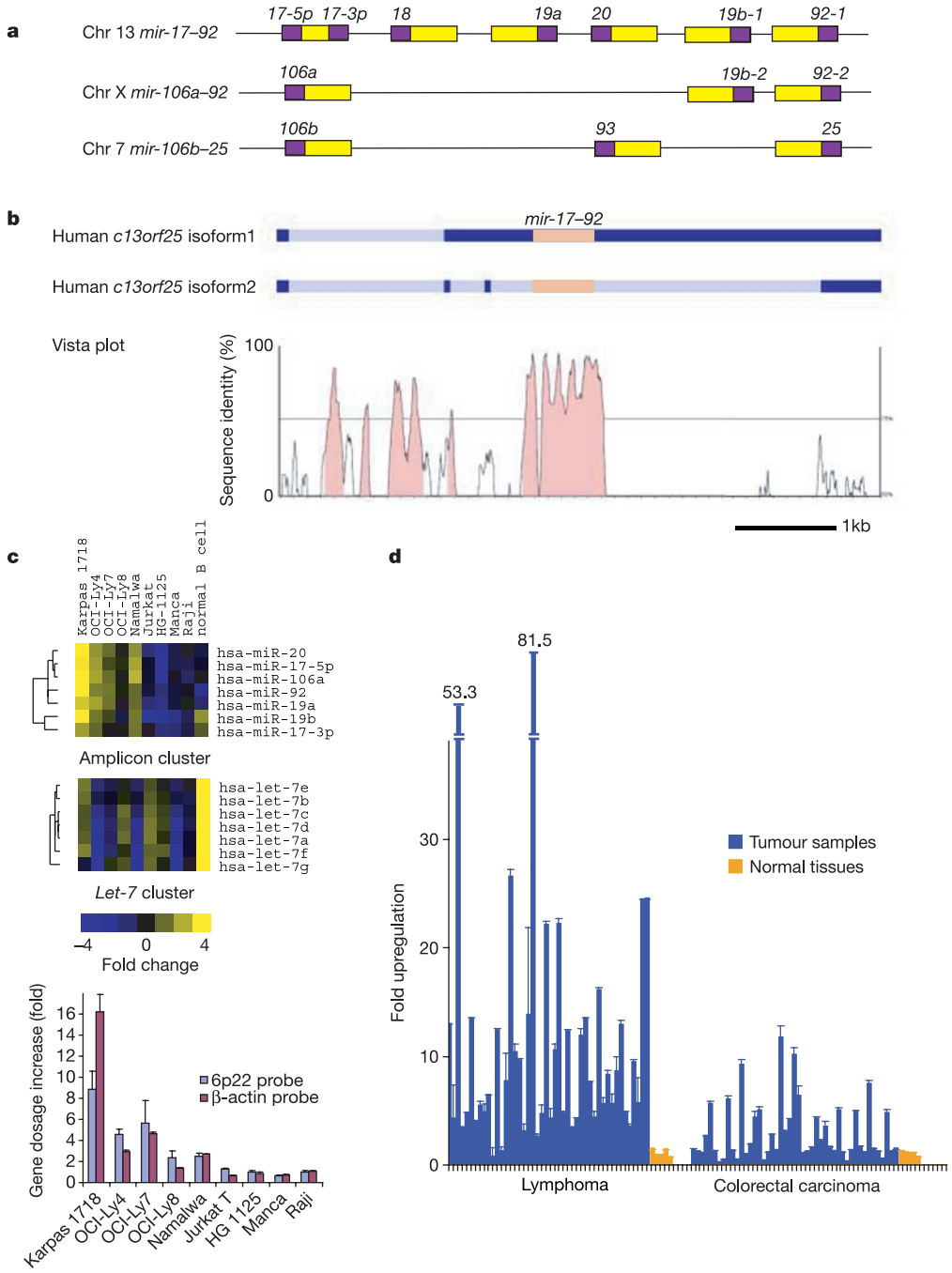

Figure 1 | The *mir-17–92* cluster shows increased expression in B-cell lymphoma samples and cell lines. **a**, Genomic organization of three polycistronic miRNA clusters is shown. There are five paralogous groups located in three homologous clusters (*mir-17–92*, *mir-106a–92* and *mir-106b–25*) with a conserved order: *miR-17-5p*/*miR-106a*/*miR-106b*; *miR-18*; *miR-19a*/*miR-19b-1*/*miR-19b-2*; *miR-20*/*miR-93*; and *miR-92-1*/*miR-92-2*/*miR-25* (yellow boxes, pre-miRNAs; purple boxes, mature miRNAs). **b**, The level of conservation between human and mouse homologues is represented using an mVista plot[28]. Two alternative isoforms have been detected for the human gene, and these are shown schematically[1] (dark blue, exons; light blue, introns; orange, the *mir-17–92* cluster). **c**, MicroRNA expression levels in cell lines carrying the 13q31-q32 amplicon (including Karpas 1718, OCI-Ly4 and OCI-Ly7) were compared to those in leukaemia and lymphoma cell lines lacking this genetic lesion, and to normal B-cells isolated from cortical blood (top panel). We included in this analysis the OCI-Ly8 cell line, which has previously been identified as a cell line carrying the 13q31-32 amplicon, but showed no gene dosage increase at the *c13orf25* locus in our study. Normalized one-channel measurements for 191 human miRNAs were hierarchically clustered for all miRNA genes represented on the array. An excerpt of the data is shown, and the full cluster analysis is presented in Supplementary Fig. 1. The expression map node that correlates with the amplification is shown. The *let-7* cluster node is also shown for comparison (middle panel). In the cell lines examined, expression levels of the mature microRNAs from the *mir-17–92* polycistron correlate with the copy number at the *mir-17–92* locus (bottom panel). **d**, The level of *mir-17–92* pri-miRNA was determined by real-time quantitative PCR in 46 lymphomas and 47 colorectal carcinomas, and compared to levels found in corresponding normal tissues from five individuals. In **c** and **d**, error bars indicate standard deviation (s.d.).

upregulation), and the degree of overexpression was substantially lower (Fig. 1d).

Considered together, our data prompted the hypothesis that *mir-17–92* might contribute to tumour development. To test this idea directly, we used a mouse model of human B-cell lymphoma. Transgenic animals carrying a *c-myc* oncogene, driven by the immunoglobulin heavy-chain enhancer (*Eμ*), develop B-cell lymphomas by 4–6 months of age[16]. Similarly, haematopoietic stem cells (HSCs) derived from fetal livers of *Eμ-myc* transgenic mice generate B-cell lymphomas with comparable latency when transplanted into lethally irradiated recipients[17–20] (Fig. 2a). We therefore infected *Eμ-myc*/+ HSCs with a murine stem cell virus (MSCV) retrovirus that directs expression of a truncated cluster comprising *mir-17–19b-1* (hereafter *mir-17–19b*), the vertebrate-specific portion of the *mir-17–92* miRNA cistron (Fig. 1a). This virus also contained a green fluorescent protein (GFP) transgene, allowing us to follow infected stem cells *in vitro* and *in vivo* (Fig. 2a). Mice reconstituted with *Eμ-myc*/+ HSCs carrying a control MSCV vector developed lymphomas after the expected latency (3–6 months), with incomplete penetrance (Fig. 2b). Similarly, we examined >40 animals reconstituted with *Eμ-myc*/+ HSCs expressing subsets of 96 different, single microRNAs (see Supplementary Table 2). Although we did not confirm miRNA overexpression for every case, we did not observe any significantly accelerated onset of disease. In contrast, 100% of the animals co-expressing the *mir-17–19b* polycistron and *c-myc* developed leukaemias at an average of 51 days following transplantation (s.d. ±13 days, $P < 0.0001$ compared with MSCV controls using the logrank test), and died of B-cell lymphomas at an average age of 65 days (s.d. ±13 days, $P < 0.0001$ compared to MSCV controls; Fig. 2b). In all but one case, primary lymphomas could be visualized by virtue of the linked GFP marker (Fig. 2c and Table 1). The mature miRNAs from the *mir-17–19b* cluster show high-level expression in these tumours, compared with miRNAs from the paralogous *mir-106a–92* locus, and also have similar *mir-17–19b* expression levels compared to the Karpas 1718 lymphoma cell line, which has increased *c13orf25* gene dosage (see Supplementary Fig. 2).

The full *mir-17–92* cistron was also tested in a small cohort of animals. Although similar results were obtained compared to those animals reconstituted with HSCs expressing *mir-17–19b*, studies in cell lines indicated that the construct used to express the entire cluster gave lower levels of mature miRNAs. We therefore focused most of our study on the truncated *mir-17–19b* cluster. In these ongoing studies, we have yet to find any individual miRNA from the

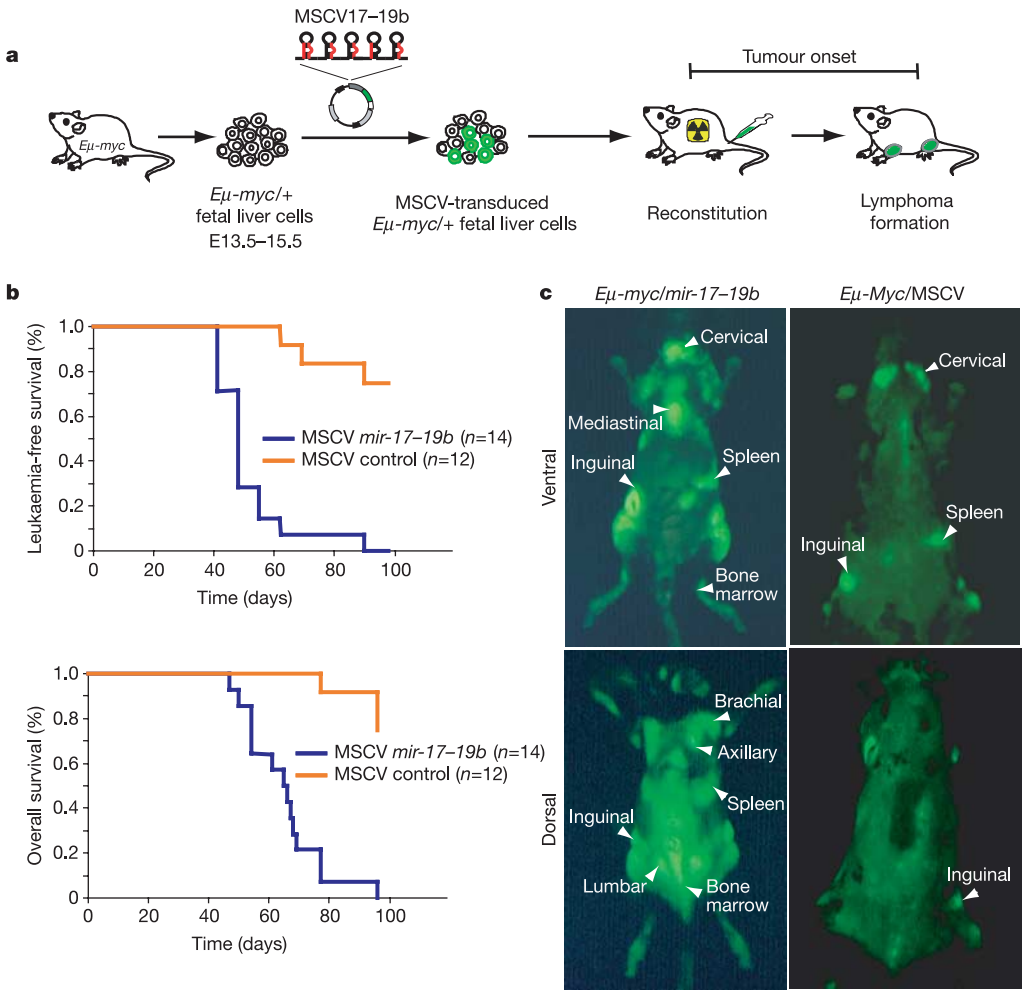

Figure 2 | Overexpression of the *mir-17–19b* cluster accelerates *c-myc*-induced lymphomagenesis in mice. **a**, Schematic representation of the adoptive transfer protocol using *Eμ-myc* HSCs. **b**, Mice reconstituted with HSCs expressing *mir-17–19b* in an MSCV retroviral vector (MSCV *mir-17–19b*) or infected with a control MSCV virus were monitored by blood smear analysis starting 5 weeks after transplantation. The Kaplan-Meier curves represent the percentage of leukaemia-free survival or overall survival. **c**, External GFP imaging of tumour-bearing mice with *Eμ-myc*/*mir-17–19b* or *Eμ-myc*/MSCV shows the overall distribution of tumour cells. *Eμ-myc*/*mir-17–19b* tumours show a more disseminated phenotype compared with control tumours. These animals are representative of their genotype.

Table 1 | Phenotypic analysis of a subset of *Eμ-myc/mir-17–19b* tumours

Animal	GFP	Immunophenotyping	Cell type	Ki67 staining	Apoptosis*	Pathological features
1	+	$B220^+$, $Thy1.2^-$, IgM^-, $CD19^+$, $CD4^-$, $CD8^-$	Pre-B cell	++(70–80%)	Low	Tumour cells invaded liver and spleen; mild infiltrations observed in lung and kidney; spleen enlarged; hindlimb paralysis
2	+	$B220^+$, $Thy1.2^{low}$, IgM^-, $CD19^+$, $CD4^-$, $CD8^-$	Pre-B cell	++(80–90%)	Low	Tumour cells invaded liver, lung and spleen; spleen enlarged
3	+	$B220^+$, $Thy1.2^-$, IgM^-, $CD19^+$, $CD4^-$, $CD8^-$	Pre-B cell	++(80–90%)	Low	Tumour cells invaded liver, lung and spleen; spleen enlarged
4	+	$B220^+$, $Thy1.2^{low}$, IgM^-, $CD19^+$, $CD4^-$, $CD8^-$	Pre-B cell	++(70–80%)	Low	Tumour cells invaded liver and spleen; spleen enlarged
5	+	$B220^+$, Thy1,2$^-$, IgM^-, $CD19^+$, $CD4^-$, $CD8^-$	Pre-B cell	++(80–90%)	Slightly less than control	Highly disseminated lymphoma; tumour cells invaded liver, spleen, lung and kidney; spleen enlarged
6	+	$B220^+$, Thy1,2$^-$, IgM^-, $CD19^+$, $CD4^-$, $CD8^-$	Pre-B cell	++(80–90%)	Low	Highly disseminated lymphoma; tumour cells invaded liver, spleen, lung and kidney; spleen enlarged
7	+	$B220^+$, $Thy1.2^-$, IgM^-, $CD19^+$, $CD4^-$, $CD8^-$	Pre-B cell	++(70–80%)	Low	Spleen enlarged; mild infiltration of tumour cells into liver only
8	+	$B220^+$, $Thy1.2^{low}$, IgM^-, $CD19^+$, $CD4^-$, $CD8^-$ and $B220^+$, $Thy1.2^{low}$, IgM^-, $CD19^+$, $CD4^-$, $CD8^-$†	Pre-B cell and mature B cell	++(70–80%)	Low	Highly disseminated lymphoma; tumour cells invaded liver, spleen, lung and kidney; enlarged spleen
9	−	ND	ND	++(80–90%)	Low	Tumour cells invaded liver, lung and spleen; enlarged spleen

*Levels of apoptosis in *Eμ-myc/mir-17–19b* lymphomas are compared to control *Eμ-myc*/MSCV lymphomas on the basis of haemotoxylin and eosin staining, and TUNEL staining.
†The two clones of tumour cells with different cell type specificity might reflect independent transformation events or maturation of a single primary clone.
ND, not determined.

mir-17–19b cluster that can accelerate tumour formation to the extent seen with the intact polycistron (not shown).

The *Eμ-myc*/*mir-17–19b* lymphomas are true malignancies rather than hyperplasias, because primary tumour cells, when transplanted into C57B6/J recipients, induce B-cell lymphomas in 2–3 weeks that result in lethality after 4–5 weeks (data not shown). The secondary tumours show pathological features indistinguishable from the original tumours, and retain tumorigenic potential after two additional rounds of serial transplantation (data not shown). Therefore, a microRNA cluster can accelerate *Eμ-myc* induced tumorigenesis in mice.

The pathological hallmarks of *Eμ-myc*/*mir-17–19b* mosaic animals included massive enlargement of lymph nodes, splenic hyperplasia, infiltration of the thymus by lymphoma cells, and leukaemia (Fig. 2c). Animals with advanced lymphomas showed extramedullary haematopoiesis due to functional failure of the bone marrow. Furthermore, 6 out of 14 animals showed hind limb paralysis, associated with substantial tumour growth at the lumbar node. Tumours resulting from combined *c-myc* and *mir-17–19b* expression consistently invaded visceral organs outside the lymphoid compartment, including liver, lung and occasionally kidney (Figs 2c, 3b and Table 1). Additionally, *Eμ-myc*/*mir-17–19b* lymphomas show a high mitotic index without extensive apoptosis (Fig. 3a). This contrasts with the *Eμ-myc*/MSCV tumours lacking the microRNA cluster, which show a high degree of apoptosis (Fig. 3a). These findings indicate that cooperation between *Eμ-myc* and *mir-17–19b* gives rise to highly malignant, disseminated lymphomas capable of evading normal apoptotic responses to inappropriate proliferation.

Eμ-myc-induced lymphomas originate from the B-lymphoid lineage. However, the developmental characteristics of these tumour cells are not stage-specific, as they can resemble either mature B cells or pre-B cells. To examine the cell lineage of the *Eμ-myc*/*mir-17–19b* lymphomas, we assessed the expression of cell-surface markers, including the B-cell-specific marker B220 and the T-cell-specific markers CD4 and CD8a. All tumours were found to be of B-cell origin, staining positive for B220 and negative for both CD4 and CD8a (Fig. 3c and Table 1). We next analysed these tumours for CD19 and IgM expression to distinguish pre-B from mature B cells. With one exception, *Eμ-myc*/*mir-17–19b* lymphomas were derived purely from the pre-B cell lineage (low to absent Thy1.2 staining, $CD19^+B220^+IgM^-$) (Table 1), suggesting that overexpression of *mir-17–19b* strongly favours transformation of B-cell progenitors under our experimental conditions.

Exactly how overproduction of *mir-17–19b* might promote oncogenesis is unclear. At a minimum, studies of tumour pathology suggest that increased expression of this cluster mitigates the pro-apoptotic response to elevated *myc* expression *in vivo*. Furthermore, we have previously shown that this miRNA cistron is highly expressed in embryonic stem cells, with expression levels decreasing during embryonic development in mice[21]. It is therefore tempting to speculate that these miRNAs promote 'stem cell' properties or specify characteristics of early developmental lineages. A detailed, mechanistic understanding of how this non-coding RNA cluster acts as an oncogene is at present hampered by the lack of a validated biochemical strategy for identifying miRNA targets.

Previous circumstantial evidence has indicated the potential involvement of a number of miRNAs in tumorigenesis. Although miRNAs only represent 1% of the mammalian genome, more than 50% of miRNA genes are located within regions associated with amplification, deletion and translocation in cancer[22]. Expression studies of various tumour types have also revealed specific alterations in miRNA profiles[22–25]. For example, *mir-15* and *mir-16* are frequently deleted and/or downregulated in B-cell chronic lymphocytic leukaemia[26], miR-143 and miR-145 show decreased abundance in colorectal neoplasia[25], and miR-155 and its non-coding RNA host gene, *BIC*, are upregulated 100-fold in Burkitt's lymphoma patients[24]. Here, we have shown that one miRNA polycistron is not only the subject of tumour-specific amplification, but that it is also overexpressed in tumours and tumour cell lines, and can act as an oncogene *in vivo*. Our results indicate that non-coding RNAs might act as integral parts of the molecular architecture of oncogene and tumour suppressor networks. Such oncogenic microRNAs might be designated 'oncomiRs, with *mir-17–92* being oncomiR-1.

METHODS

miRNA expression profiling. Five micrograms of total RNA was labelled with RNA ligase and a Cy3-conjugated dinucleotide, and hybridized to custom oligonucleotide microarrays as described in ref. 21. Cy3 median intensity values

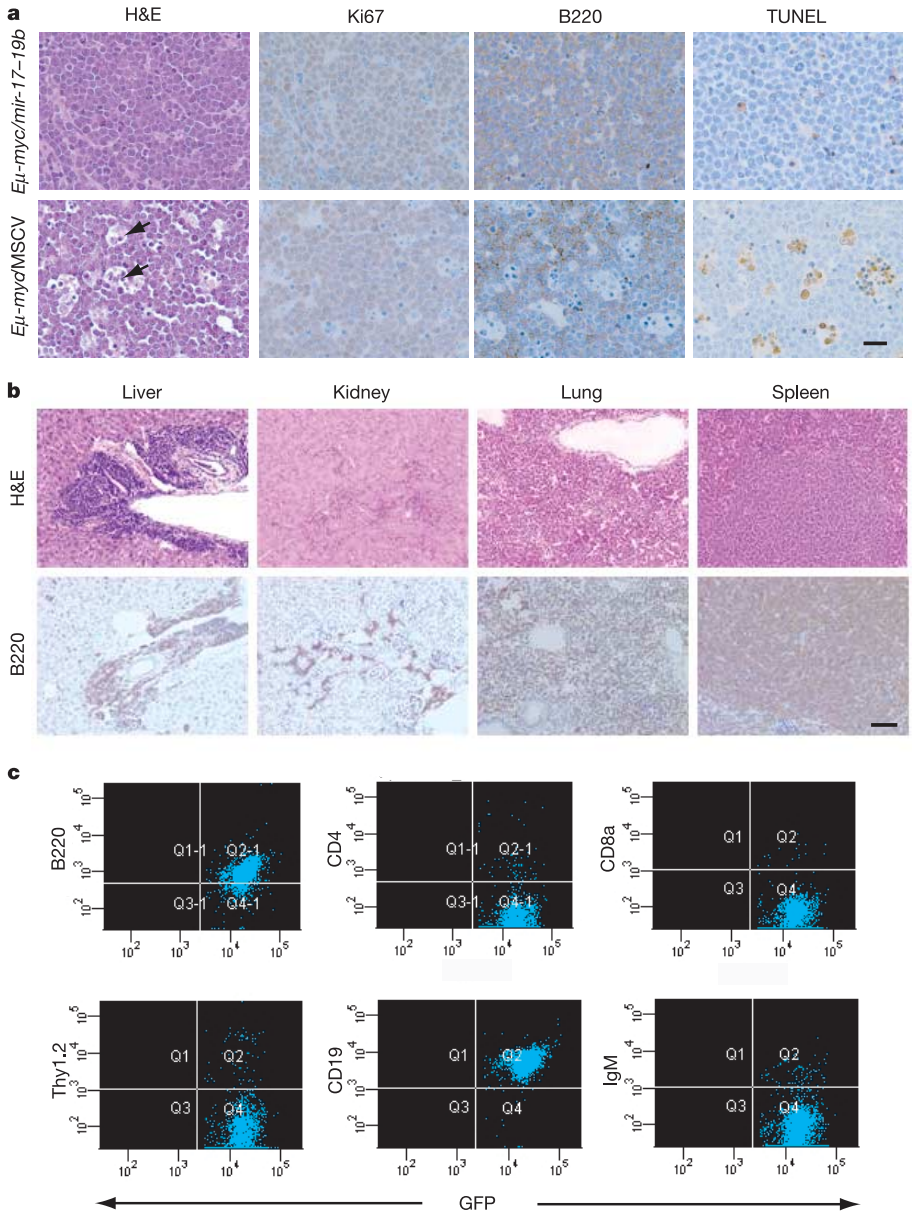

Figure 3 | Pathological and immunological analysis of lymphomas produced by cooperation between *mir-17–19b* and *c-myc*. **a**, Haemotoxylin and eosin (H&E), Ki67, B220 and TUNEL staining of *Eμ-myc/mir-17–19b* lymph node tumours. The 'starry sky' morphology is a hallmark of cell clusters undergoing apoptosis (black arrows). Scale bar, 10 μm. **b**, Invasion of visceral organs (liver, spleen, lung and kidney) by *Eμ-myc/mir-17–19b* tumour cells, shown by H&E and B220 staining. Invasion was observed both perivascularly and parenchymally in liver. Scale bar, 50 μm. **c**, Immunophenotyping of *Eμ-myc/mir-17–19b* lymphomas. Tumour cells stained positively for the B-cell-specific marker B220, but not for the T-cell-specific markers CD4, CD8a and Thy1.2. Tumour cells bore cellular characteristics of pre-B cells, staining positively for CD19 but not for IgM, a marker of mature B-cells.

were filtered to remove data points that did not exceed background levels by twofold. Values were $\log_2$-transformed and median-centred by array. Clustering was performed with Cluster (Stanford University), using values that were median-centred by gene. Dendrograms and expression maps were generated using Treeview (Stanford).

Cell lines. The measurement of miRNA abundance was carried out using the following human cell lines: Karpas 1718 (derived from splenic lymphoma with villous lymphocytes, provided by A. Karpas), OCI-Ly4, OCI-Ly7 and OCI-Ly8 (derived from diffuse large B-cell lymphoma, provided by R. Dalla-Favera). The cell lines lacking the 13q31-q32 amplicon were Raji (B-cell, derived from Burkitt's lymphoma, ATCC); Namalwa (B-cell, derived from Burkitt's lymphoma, ATCC); HG 1125 (EBV-transformed human lymphoblastoid, provided by B. Stillman); Manca (lymphoblast-like, derived from chronic myelogenous leukaemia); Jurkat; proliferating B-cells (spleenic B-cells isolated from a C57B6/Ly5.2 mouse and stimulated to proliferate in culture with lipopolysaccharide, provided by I. Weissman); and normal B cells (derived from cord blood, Cambrex).

PCR and copy number analysis. Tumour samples were obtained from the Cooperative Human Tissue Network (http://www-chtn.ims.nci.nih.gov). Corresponding normal tissue RNA from five individuals was purchased from Biochain Institute Inc. For fluorogenic real-time PCR, primers that amplify *mir-17–92* pri-miRNA and *β-actin* mRNA (control), and probes were designed using Primer Express software (V.2): *mir-17–92* forward primer, 3′-CAGTAAA GGTAAGGAGAGCTCAATCTG-5′; reverse primer, 3′-CATACAACCACTAA GCTAAAGAATAATCTGA-5′; *mir-17–92* probe, (6-FAM)-TGGAAATAAGATC ATCATGCCCACTTGAGAC-(TAMRA); *β-actin* forward primer, 3′-GCAAAG ACCTGTACGCCAACA-5′; reverse primer, 3′-TGCATCCTGTCGGCAATG-5′; *β-actin* probe, (6-FAM)-TGGCGGCACCACCATGTACC-(TAMRA). The ratios of RNA species detected by *mir-17–92* primers and *β-actin* primers in each RNA sample were determined in triplicate by reverse-transcription, quantitative PCR

using an ABI 7900HT Taqman sequence detector, following the 'standard curve' method. All values were subsequently normalized to the averaged ratio of the five corresponding normal samples. For DNA copy number determination using the ABI 7900HT sequence detector, we performed quantitative PCR analysis using the same *mir-17–92* primer set described above, and normalized the data against a reference probe corresponding to chromosomal region 6p22 (forward primer, 3′-GGTCTCTATTTGCACTTGGCTGAT-5′; reverse primer, 3′-TTTTCA TTGTTGACCAAGCTAGACA-5′; probe, (6-FAM)-TAGGGCATACTGCCTG CATATTTCCTGCT-(TAMRA)) or a *β-actin* probe. The reported values represent the ratios of DNA copy number at the *mir-17–92* locus to the normal reference probe.

Adoptive transfer of *Eμ-myc* HSCs. Fetal liver-derived HSCs were isolated from *Eμ-myc*/+ mouse embryos at embryonic day (E)13.5–E15.5, and were transduced with MSCV alone or MSCV expressing the *mir-17–19b* cluster. To exclude the possibility that the observed acceleration of lymphomagenesis was due to insertional mutagenesis, independent experiments were carried out using fetal liver cells isolated from eight *Eμ-myc*/+ embryos. Cells from each isolation were separately infected with MSCV *mir-17–19b* or control MSCV. The MSCV retroviral vector used in our studies contains a PGK-puromycin-IRES-GFP (PIG) cassette[18]. Infection rates, assessed by fluorescence-activated cell sorting (FACS), were typically 40% of bulk fetal liver cells. HSCs infected with MSCV-*mir17–19b*-PIG and MSCV-PIG (control) were subsequently transplanted into 6–8-week-old, lethally irradiated C57BL/6 recipient mice[17]. Tumour onset was monitored by blood smear analysis, and tumour samples were either collected into 4% paraformaldehyde for histopathological studies, or prepared as single-cell suspensions for FACS.

We also carried out a screen of 96 miRNAs, to look for miRNA(s) that accelerate Myc-induced lymphomagenesis. In this experiment, each pre-miRNA (and ~50 bp of flanking sequence 5′ and 3′ of the pre-miRNA) was cloned downstream of the cytomegalovirus (CMV) promoter in a MSCV vector containing SV40–GFP. Eight individual MSCV constructs, each overexpressing a specific miRNA, were pooled at equal concentrations. Twelve pools of DNA were used individually to produce virus to infect *Eμ-myc*/+ fetal liver cells for adoptive transfer into at least three recipient animals, as described above. Recipient animals were monitored for tumour growth for at least six months. For those that developed lymphoma, tumour cells were prepared from the enlarged lymph nodes and then subjected to FACS analysis for GFP expression.

Histopathology. Tissue samples were fixed in 4% paraformaldehyde, embedded in paraffin, sectioned into 5-μm slices, and stained with haemotoxylin and eosin. For Ki67 detection (rabbit anti-Ki67 antibody, NovoCastra), representative sections were deparaffinized, rehydrated in graded alcohols, and processed using the avidin–biotin immunoperoxidase method. Sections were then subjected to antigen retrieval by microwave oven treatment using standard procedures. Diaminobenzidine was used as the chromogen and haematoxylin as the nuclear counterstain. For B220 immunohistochemistry, a rat anti-mouse CD45R/B220 antibody (clone RA3-6B2, BD Biosciences Pharmingen) was used; pretreatment for antigen retrieval was not required. Analysis of the rate of apoptotis by TUNEL assay was performed according to a published protocol[27].

Received 15 February; accepted 16 March 2005.

1. Ota, A. *et al.* Identification and characterization of a novel gene, *C13orf25*, as a target for 13q31-q32 amplification in malignant lymphoma. *Cancer Res.* **64,** 3087–3095 (2004).
2. Lee, Y. *et al.* The nuclear RNase III Drosha initiates microRNA processing. *Nature* **425,** 415–419 (2003).
3. Bernstein, E., Caudy, A. A., Hammond, S. M. & Hannon, G. J. Role for a bidentate ribonuclease in the initiation step of RNA interference. *Nature* **409,** 363–366 (2001).
4. Bartel, D. P. MicroRNAs: genomics, biogenesis, mechanism, and function. *Cell* **116,** 281–297 (2004).
5. Ambros, V. The functions of animal microRNAs. *Nature* **431,** 350–355 (2004).
6. He, L. & Hannon, G. J. MicroRNAs: small RNAs with a big role in gene regulation. *Nature Rev. Genet.* **5,** 522–531 (2004).
7. Ruvkun, G. & Giusto, J. The *Caenorhabditis elegans* heterochronic gene *lin-14* encodes a nuclear protein that forms a temporal developmental switch. *Nature* **338,** 313–319 (1989).
8. Ambros, V. A hierarchy of regulatory genes controls a larva-to-adult developmental switch in *C. elegans*. *Cell* **57,** 49–57 (1989).
9. Chang, S., Johnston, R. J. Jr, Frokjaer-Jensen, C., Lockery, S. & Hobert, O. MicroRNAs act sequentially and asymmetrically to control chemosensory laterality in the nematode. *Nature* **430,** 785–789 (2004).
10. Johnston, R. J. & Hobert, O. A microRNA controlling left/right neuronal asymmetry in *Caenorhabditis elegans*. *Nature* **426,** 845–849 (2003).
11. Brennecke, J., Hipfner, D. R., Stark, A., Russell, R. B. & Cohen, S. M. *bantam* encodes a developmentally regulated microRNA that controls cell proliferation and regulates the proapoptotic gene *hid* in *Drosophila*. *Cell* **113,** 25–36 (2003).
12. Chen, C. Z., Li, L., Lodish, H. F. & Bartel, D. P. MicroRNAs modulate hematopoietic lineage differentiation. *Science* **303,** 83–86 (2004).
13. Knuutila, S. *et al.* DNA copy number amplifications in human neoplasms: review of comparative genomic hybridization studies. *Am. J. Pathol.* **152,** 1107–1123 (1998).
14. Tanzer, A. & Stadler, P. F. Molecular evolution of a microRNA cluster. *J. Mol. Biol.* **339,** 327–335 (2004).
15. Tusher, V. G., Tibshirani, R. & Chu, G. Significance analysis of microarrays applied to the ionizing radiation response. *Proc. Natl Acad. Sci. USA* **98,** 5116–5121 (2001).
16. Adams, J. M. *et al.* The *c-myc* oncogene driven by immunoglobulin enhancers induces lymphoid malignancy in transgenic mice. *Nature* **318,** 533–538 (1985).
17. Schmitt, C. A. *et al.* Dissecting p53 tumor suppressor functions *in vivo*. *Cancer Cell* **1,** 289–298 (2002).
18. Hemann, M. T. *et al.* An epi-allelic series of p53 hypomorphs created by stable RNAi produces distinct tumor phenotypes *in vivo*. *Nature Genet.* **33,** 396–400 (2003).
19. Hemann, M. T. *et al.* Suppression of tumorigenesis by the p53 target PUMA. *Proc. Natl Acad. Sci. USA* **101,** 9333–9338 (2004).
20. Wendel, H. G. *et al.* Survival signalling by Akt and eIF4E in oncogenesis and cancer therapy. *Nature* **428,** 332–337 (2004).
21. Thomson, J. M., Parker, J., Perou, C. M. & Hammond, S. M. A custom microarray plateform for analysis of microRNA gene expression. *Nature Methods* **1,** 47–53 (2004).
22. Calin, G. A. *et al.* Human microRNA genes are frequently located at fragile sites and genomic regions involved in cancers. *Proc. Natl Acad. Sci. USA* **101,** 2999–3004 (2004).
23. Calin, G. A. *et al.* MicroRNA profiling reveals distinct signatures in B cell chronic lymphocytic leukemias. *Proc. Natl Acad. Sci. USA* **101,** 11755–11760 (2004).
24. Metzler, M., Wilda, M., Busch, K., Viehmann, S. & Borkhardt, A. High expression of precursor microRNA-155/*BIC* RNA in children with Burkitt lymphoma. *Genes Chromosom. Cancer* **39,** 167–169 (2004).
25. Michael, M. Z., O'Connor, S. M., van Holst Pellekaan, N. G., Young, G. P. & James, R. J. Reduced accumulation of specific microRNAs in colorectal neoplasia. *Mol. Cancer Res.* **1,** 882–891 (2003).
26. Calin, G. A. *et al.* Frequent deletions and down-regulation of micro- RNA genes *miR15* and *miR16* at 13q14 in chronic lymphocytic leukemia. *Proc. Natl Acad. Sci. USA* **99,** 15524–15529 (2002).
27. Di Cristofano, A., De Acetis, M., Koff, A., Cordon-Cardo, C. & Pandolfi, P. P. Pten and $p27^{KIP1}$ cooperate in prostate cancer tumor suppression in the mouse. *Nature Genet.* **27,** 222–224 (2001).
28. Mayor, C. *et al.* VISTA: visualizing global DNA sequence alignments of arbitrary length. *Bioinformatics* **16,** 1046–1047 (2000).

Supplementary Information is linked to the online version of the paper at www.nature.com/nature.

Acknowledgements We thank members of the Hannon, Lowe and Hammond laboratories for discussions and input. We also thank Z. Xuan, N. Chen, N. Sheth and R. Sachidanandam for bioniformatic analysis. C. Perou and J. Leib provided advice and support for microarray methodologies, and A. Barnes and B. Boone gave assistance with mouse tissue procurement. We are grateful to H. Wendel, C. Scott, C. Marsden and C. Rosenthal, R. Karni, P. Moody and R. Whitaker, who provided advice and technical support. F. Slack coined the oncomiR nomenclature. L.H. and M.T.H. are Fellows of the Helen Hay Whitney Foundation. S.W.L. and C.C.-C. are supported by a program project grant from the NCI. G.J.H is supported by an Innovator Award from the US Army Breast Cancer Research Program and by grants from the DOD and NIH. S.M.H. is a General Motors Cancer Research Foundation Scholar, and J.M.T is a Frederick Gardner Cottrell Postdoctoral Fellow.

Author Information Microarray data have been deposited in NCBI-GEO under accession numbers GSM45026–GSM45065 and GSE-2399. Reprints and permissions information is available at npg.nature.com/reprintsandpermissions. The authors declare no competing financial interests. Correspondence and requests for materials should be addressed to G.J.H. (hannon@cshl.edu) or S.M.H. (hammond@med.unc.edu).